Understanding CO_2 adsorption in a flexible zeolite through a combination of structural, kinetic and modelling techniques

Maarten C. Verbraeken[1], Roberto Mennitto[1], Veselina M. Georgieva[2], Elliott L. Bruce[2], Alex G. Greenaway[2], Paul A. Cox[3], Jung Gi Min[4], Suk Bong Hong[4], Paul A. Wright[2], Stefano Brandani[1*]

[1]School of Engineering, University of Edinburgh, The King's Buildings, Edinburgh, United Kingdom

[2]EaStCHEM School of Chemistry, University of St Andrews, Purdie Building, North Haugh, St Andrews, United Kingdom

[3]School of Pharmacy and Biomedical Sciences, University of Portsmouth, Portsmouth, United Kingdom

[4]Center for Ordered Nanoporous Materials Synthesis, Division of Environmental Science and Engineering, POSTECH, Pohang, Korea

Abstract

In this study we show how non-trivial equilibrium and kinetic adsorption behaviour in a flexible zeolite can be understood through a combination of experimental characterisation and modelling. Flexible zeolites, such as those in the RHO-family, can exhibit unusual stepped isotherms in the presence of CO_2, but their structural complexity makes it hard to attribute a clear mechanism. Here we present a structural and kinetic study on (Na,TEA)-ZSM-25, an extended member of the RHO-family, and show that by combining diffraction data, lattice fluid modelling and dynamic column experiments, we obtain a plausible mechanism for CO_2 adsorption and transport in this material. It is evident that by using any single technique, the behaviour is too complex to be readily understood. This is to our knowledge the first study to measure and model the changing kinetics due to adsorption induced framework flexibility.

Keywords: ZSM-25, Adsorption, Synchrotron X-ray diffraction, Zero Length Column technique, Lattice Fluid

* Corresponding author: s.brandani@ed.ac.uk

Introduction

Gas separation by means of adsorption is versatile, robust and highly scalable and this technology is therefore widely applied industrially. Zeolite adsorbents have made important contributions in this area over many decades[1], including application in non-cryogenic air separation, where Li-forms of the large pore zeolite X are among the most efficient for N_2/O_2 separation[2] and in hydrogen purification, where removal of CO_2, CO and CH_4 from steam reformate of methane can be achieved using zeolites NaX and NaA, among other adsorbents[3].

One particularly promising use of zeolite adsorbents of great current interest is the selective adsorption of carbon dioxide, carbon capture, for instance from natural or biogas feeds or effluent streams in power plants, leading to plant efficiency gains and reductions in greenhouse gas emissions, respectively. For this application, the variable polarity of zeolites can be tuned to control selectivity and ease of regeneration[4]. Furthermore, small pore zeolites (with window sizes below 4Å) offer enhanced CO_2/CH_4 selectivity via molecular sieving effects, and so there has been increased interest in such materials of late, including zeolite A and its higher Si/Al variant ZK-4, and zeolites Rho, chabazite and ZK-5[5–10].

Until quite recently, adsorbents were assumed to be inert and rigid hosts to the small gas molecules they take up, although changes in the structure of zeolites upon uptake of large organic molecules have long been known and have recently been found to affect sorbate diffusivity[11–13]. With the advent of advanced materials for gas separation and new insights into their molecular workings, it has become apparent that the adsorbents themselves can undergo significant changes during the process of adsorption of small gas molecules[14–17]. These structural changes occur via a number of different mechanisms that range from simple framework expansion and contraction to more remarkable behaviour such as breathing and gate-opening[18]. Although these changes have been studied most widely in metal organic frameworks (MOFs), such effects are increasingly observed in materials which are considered 'rigid', such as zeolites[14,16,19–21].

In 'breathing' metal organic frameworks (MOFs), such as the 'wine-rack' structure MIL-53[22], the structure opens in response to CO_2 uptake to give a much larger unit cell and a correspondingly higher specific pore volume. This expansion occurs in response to changes in the balance of dispersive forces between adjacent organic linkers and those between the MOF and the adsorbate molecules, and are made possible by the many degrees of configurational freedom enjoyed by the linker molecules and their hinged linkages to metal-based nodes. In aluminosilicate zeolites, by contrast, diverse adsorption-related phenomena can result from the modulation of the coulombic interaction of the negatively-charged frameworks with extra-framework cations by uptake of polar or polarisable adsorbates[20,23]. If the cations are located in windows that guard access to the pore space, then cation gating can occur, where only certain strongly interacting molecules can enter. Alternatively, for zeolites that possess flexible frameworks that are able to adapt upon dehydration to achieve improved coordination with extra-framework cations (usually resulting in smaller window sizes), then cation-adsorbate interactions upon uptake of polar molecules results in weakening cation-framework interactions and subsequent framework relaxation, which increases window and pore size in a type of structural breathing. While gating effects can afford enhanced selectivity, by only allowing certain molecules to enter a solid's micropores,[16,23,24] structural breathing could provide a large working capacity over a small pressure range, particularly in pressure swing adsorption processes[25,26]. To assess whether the controllable flexibility of such zeolitic adsorbents can be applied within next generation adsorptive processes, more understanding of the mechanism of their behaviour is required, as well as accurate quantitative models describing their thermodynamic and kinetic performance under realistic conditions.

Here we consider (Na,TEA)-ZSM-25 (TEA = tetraethylammonium cations, remaining encapsulated after crystallisation), a member of the zeolite RHO family. This family of small pore zeolites, where access to the pore space is limited by 8R windows (bounded by rings containing 8 framework cations), has received increased attention recently, due to their relatively high CO_2 capacity and promising selectivity for CH_4/CO_2 separation[27]. Na-Rho has excellent CO_2 capacity, but suffers from poor transport kinetics, limiting its usefulness in an industrial process[16]. Higher generation RHO family members (PST-29, ECR-18, ZSM-25, PST-20…) make up a series of isoreticular embedded zeolite structures, where interpenetrated scaffolds of *lta-(d8r-pau)$_n$-d8r-lta* cages (n = 0, 1, 2, 3…) are separated by embedded cages (*t-oto, t-plg, t-gsm and t-phi*) so that all micropore space is accessible via 8Rs[27,28]. The framework structure of ZSM-25 is illustrated in Figure 1.

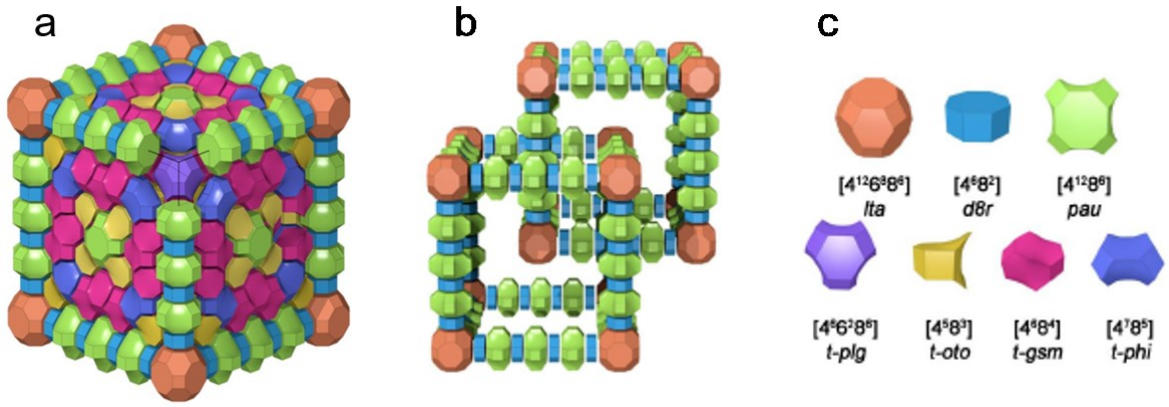

Figure 1: Structure of ZSM-25, represented as a 3D tiling of cages, each linked to others via 8R windows (a). The structure can be envisaged as interpenetrating scaffolds (b) of lta, d8r and pau cages, with the remaining space occupied by embedded cages of t-plg, t-oto, t-gsm and t-phi. The cage types are illustrated in (c). In one unit cell of the ZSM-25 structure there are 2 lta, 24 d8r, 18 pau, 24 t-plg, 144 t-oto, 60 t-gsm and 72 t-phi cages. Each edge of a tile represents a T-O-T linkage (T = Si,Al). Adapted with permission from [ref.[27]]. Copyright 2015 Nature Publishing Group.

All of these RHO-n structures display framework flexibility as observed by changes of the unit cell upon dehydration, although for higher members than ECR-18 the dehydrated structures have not been reported.[29,30] Initial adsorption measurements showed the higher generation RHO-n structures exhibited much faster adsorption kinetics than Rho, which may be attributed to faster diffusion of CO_2 through the 'embedded'' cages rather than through the scaffold. Furthermore, a detailed study of adsorption of CO_2 in univalent cation forms of both the as-prepared (Na,TEA)-ZSM-25 and the calcined and exchanged Na-ZSM-25 showed stepped isotherms without hysteresis, characteristic of structural changes. Furthermore, (Na,TEA)-ZSM-25 was shown to be a promising material for CO_2/CH_4 separation, even at elevated CH_4 pressures.

As mentioned, good transport properties are essential for a material's utilisation in industrial separation processes. One method of estimating these properties in a microporous solid is the zero length column (ZLC) technique[31,32]. The technique typically involves measuring the desorption of a previously saturated sample after a step change in the gas phase concentration. Kinetic information can be extracted by fitting the experimental data to a theoretical model, in which the relevant molecule's diffusivity through the zeolite structure is a model parameter. This methodology has been used to great effect on a number of materials in various atmospheres[33–35], but it is usually limited to systems exhibiting type I isotherms, a key modelling assumption[36]. Materials exhibiting

stepped isotherms, resulting from framework flexibility, therefore present a challenge in analysing ZLC data; indeed, difficulties were encountered when fitting ZLC data on Na-RHO at CO_2 partial pressures over 0.01 bar, due to non-type I behaviour under these conditions[16].

Recently, we published isotherm predictions by a new thermodynamic framework, the Rigid Adsorbent Lattice Fluid (RALF)[37]. A key characteristic of RALF is the fact that it allows for structural changes within the solid and thus inherently accounts for any effects this may have on its isotherms. The model's effectiveness was demonstrated through accurate predictions of the adsorption behaviour of MIL-53 (Al), a breathing MOF exhibiting steps in its isotherms due to dramatic volume changes[38]. In this contribution we will first model the stepped isotherms of (Na,TEA)-ZSM-25 through RALF. In order to minimise modelling parameters and ensure it physically represents the adsorption behaviour of the adsorbent, we utilise a suite of structural and physical characterisation techniques to parameterise our model. This equilibrium model can subsequently be used to simulate the desorption profile of a ZLC experiment with a minimum of fitting parameters, allowing to extract kinetic information on this flexible material. The adsorption characteristics derived from the RALF modelling are put into the context of the flexible framework structure of ZSM-25 that is derived from experimental diffraction studies.

Experimental

Materials

(Na,TEA)-ZSM-25 was synthesised by a hydrothermal route as previously reported and confirmed in the literature [27,39]. The starting gel mixture with composition 2.6 TEA_2O·1.9 Na_2O·1.0 Al_2O_3·7.2 SiO_2·390 H_2O was prepared by dissolving aluminium hydroxide ($Al(OH)_3$·1.0H_2O, Aldrich, 1.92 g) and sodium hydroxide (NaOH, Fisher chemicals, 99.25 wt.%, 1.52 g) in deionized water (63.25 g). Tetraethylammonium bromide (TEABr, Aldrich, 98%, 11.15 g) and colloidal silica, Ludox AS-40 (SiO_2, Aldrich, 40 wt.% in water, 10.8 g) were slowly added to the aluminium/sodium hydroxide solution whilst stirring thoroughly until homogeneous. The as-prepared gel was aged at room temperature for 24 h in a closed polypropylene bottle under continuous stirring. The final synthesis mixture was transferred to a PTFE-lined stainless-steel autoclave and hydrothermally treated at 408 K for 7 days under slow rotation (60 rpm). After allowing the autoclave to cool to room temperature, the product was filtered and washed with distilled water until the pH value of the filtrate was about 8. After washing, all samples were dried at 373 K for 12 h and used for characterization.

Structural characterisation

Powder X-ray diffraction (PXRD) patterns of the synthesised (Na,TEA)-ZSM-25 were initially measured in flat plate Bragg-Brentano reflection geometry, $\theta - 2\theta$ mode, at room temperature, on a PANalytical Empyrean diffractometer with a Cu X-ray tube (Cu $K_{\alpha 1}$) and X'celerator RTMS detector.

Synchrotron powder X-Ray diffraction (PXRD) patterns of as-prepared (Na,TEA)-ZSM-25 and calcined (Na,H)-ZSM-25 were collected at room temperature at beamline I11 at the Diamond Light Source (λ = 0.826956 Å), Harwell and ID31 at the ESRF (λ = 0.320012 Å), Grenoble, respectively. Powdered as-prepared (Na,TEA)-ZSM-25 was placed in a 0.7 mm quartz glass capillary and evacuated and dehydrated at 500 K for 2 h under a dynamic vacuum of 10^{-5} mbar. This sample was subsequently exposed to CO_2 gas and left to equilibrate for 20 min before data collection. Separately, a sample of (Na,H)-ZSM-25 was prepared by calcination of Na,TEA-ZSM-25 for 12 h at 823 K and loaded in a 0.7

mm quartz glass capillary, dehydrated at 573 K for 6 h at 10^{-5} mbar and flame sealed before being analysed at ID31.

Rietveld refinements were carried out using TOPAS Academic V6 software, using frameworks optimised through molecular modelling with similar unit cell sizes as starting models. Geometric restraints of T-O and O-O of 1.63 and 2.63 Å, respectively, were applied. Initial extra-framework cation positions and occupancies were chosen based on literature positions and allowed to refine and adapted where necessary using difference Fourier analysis. Pseudo-Voigt peak profiles were found to be the best fit of those available. A minor impurity of PST-20 was fitted in the as-prepared data, with only the lattice parameter refined. The structural model for the dehydrated PST-20 impurity was obtained by a method similar to that used for ZSM-25 (described in the Results section) and will be described elsewhere.

Variable pressure X-ray diffraction experiments were performed on a PANalytical Empyrean diffractometer with a Mo X-ray tube with a ß-filter (giving Mo $K_{\alpha 1,2}$ X-radiation) and an X'celerator RTMS detector. The instrument was equipped with an Anton Paar HTK1200N stage (room temperature - 1200°C, up to 1 bar pressure of inert/reducing gas), working in reflection, Bragg Brentano, θ – θ mode. First, the sample was placed on an alumina disk and inserted in a cell, equipped with a furnace. The sample was evacuated and degassed for 16 h under a vacuum of 10^{-6} mbar at 500 K. The furnace was attached to a dosing rig made of 1/8" stainless steel line and a needle valve, used to dose the CO_2 supply. The pressure was followed on a RS PRO vacuum gauge with a maximum pressure measurement of 0 bar overpressure (1 bar absolute pressure). Series of diffraction patterns, each of 60 min and over the 2θ range 3.5-25°, were collected at 298 K and 328 K before and after dehydration, and also after dosing with 0.02, 0.04, 0.06, 0.08, 0.10, 0.20, 0.30, 0.40, 0.60, 0.80 and 1.0 bar of CO_2, respectively, always allowing for 60 min of equilibration.

The crystal size and morphology of the samples were studied by scanning electron microscopy (SEM). Electron micrographs were taken on a JEOL JSM-6700F equipped with a field emission gun (FEG) electron source. The as-prepared (Na,TEA)-ZSM-25 material has a uniform crystal size of 1 – 2 μm as seen in Figure S1 in the supporting information.

Thermogravimetry (TG) of (Na,TEA)-ZSM-25 zeolite was performed using a Netzsch TG 209 instrument with a heating rate of 3 K min^{-1} up to 1173 K in flowing air, in order to determine the temperature at which water and template were released. As shown in Figure S2 in the supporting information, the templated material continuously loses weight between room temperature and 900 K. To avoid decomposition of the template during regeneration/activation of the sample, heat treatments were limited to 500 K.

Physical characterisation

He pycnometry

He pycnometry was performed using an Ultrapyc 1200e (Quantachrome Instruments), equipped with a small sample cell. Prior to performing the measurements, the (Na,TEA)-ZSM-25 sample was heated overnight to 473 K under vacuum. After cooling down, the sample was left in a Helium (BOC, CP grade, 99.999% purity and additionally dried through columns packed with a combination of silica gel and zeolite 5A molecular sieve) atmosphere and its weight recorded. This sample, with mass 0.13338 g, was subsequently introduced into the sample cell, after which the pycnometry was carried out, between atmospheric pressure and 2.2 bar at room temperature. Eight consecutive runs were performed with a maximum volume deviation of 1.2 %. For added accuracy, prior to measuring

the sample, a calibration of the sample cell was performed using stainless steel beads with a volume close to that of the sample. The calculated skeletal density of the sample was found to be 2640 kg m^{-3}.

CO_2 isotherms

CO_2 (BOC, 99.8% purity) adsorption isotherms on (Na,TEA)-ZSM-25 powder were measured on the volumetric Autosorb iQ system (Quantachrome Instruments) at 268 K, 288 K, 308 K and 328 K. First, the weight of an empty 9 mm measuring cell with sealing plug was recorded. The sample was then inserted into the measuring cell and heated overnight at 473 K in vacuum. After backfilling with helium and replacing the plug, the sample plus measuring cell was recorded; the difference between the two weights provided the sample mass, i.e. 0.1041 g. Isotherms were subsequently recorded using the instrument's standard mode, which involves dosing the adsorbate gas several times until a pre-specified equilibrium pressure is reached. The tolerance for pressure changes over a 15 minute period was set to the minimum possible to ensure equilibrium was reached for each point. Adsorption isotherms were measured up to 100 kPa; desorption isotherms were measured down to 50 Pa. The measurements were controlled by the ASiQwin software and sample temperature was maintained by a water bath connected to a Julabo F-25 recirculator. The gases used during the measurements were pre-dried using columns packed with a combination of silica gel and zeolite 5A molecular sieve.

Kinetic experiments

The ZLC experimental setup is described in great detail in ref.[40] In summary, a small amount (~ 5 mg) of (Na,TEA)-ZSM-25 sample was packed into a 1/8" stainless steel union (Swagelok®), fitted with two porous metal discs to keep the powder in place. The column and gas connections are placed either within an oven (Carbolite) with thermostatic control (Eurotherm) or inside a cooling jacket, connected to a thermostatic bath for temperature control (Julabo F-25). The pure helium carrier and dosing gas mixtures (10 – 20 vol.% CO_2 in helium) are supplied through mass flow controllers (Brooks Instrument) and a combination of four solenoid valves is used to direct either of the two gas streams to the ZLC. Both helium (BOC, CP grade, 99.999% purity) and CO_2 (BOC, 99.8% purity) are additionally dried using columns packed with a combination of silica gel and zeolite 5A molecular sieve. The gas leaving the ZLC is analysed by mass spectrometry (Dycor Residual Gas Analyzer, Ametek Process Instruments). Prior to ZLC measurements, the sample was activated overnight at 473 K under a flow of helium.

Theory

The Rigid Adsorbent Lattice Fluid

The Rigid Adsorbent Lattice Fluid (RALF) model has been described in great detail in refs. [37,38] It was shown that the model can accurately describe and predict equilibrium adsorption behaviour in both *'frozen'* as well as flexible adsorbents, with a minimum of modelling parameters. The equilibrium behaviour of the system is derived through the residual Gibbs energy, which for a single adsorbate is given by equation 1. Here we opt for the chemical engineering nomenclature as used in various textbooks, where the term residual refers to the departure of a thermodynamic property from that of an ideal gas at the same temperature and pressure[41,42] .

$$\frac{G^R(T,P,N)}{RT} = rN\left[-\frac{\tilde{\rho}}{\tilde{T}} + \frac{(1-\tilde{\rho})\ln(1-\tilde{\rho})}{\tilde{\rho}} + 1\right] + N(z - 1 - \ln z) \quad (1)$$

Equation 1 is the expression for the residual Gibbs energy of the adsorbed phase given in ref.[37] written for a single adsorbate, given that the combinatorial term for a single adsorbate becomes zero due to the crystalline nature of the solid. The reduced quantities are defined by:

$$\tilde{T} = \frac{T}{T^*} \qquad \tilde{P} = \frac{P}{P^*} \qquad \tilde{\rho} = \frac{\rho}{\rho^*}$$

Where T^*, P^* and ρ^* are the characteristic temperature, pressure and density of the lattice fluid. N is the total number of moles in the system and r is the overall number of lattice sites per molecule. The compressibility factor is as usual, i.e. $z = \frac{PV}{NRT} = r\frac{\tilde{P}}{\tilde{\rho}\tilde{T}}$.

Through the residual Gibbs energy we can determine the adsorbed and fluid phase chemical potentials by carrying out the derivations with respect to number of moles of component *k*, i.e.

$$\frac{{\mu_k}^R}{RT} = \frac{1}{RT}\left(\frac{\partial G^R}{\partial N_k}\right)_{T,P,N_{j\neq k}} = \ln\varphi_k$$

For the calculation of adsorption isotherms, we can now use the usual equilibrium condition, which is for the chemical potentials of component *k* to be equal in the adsorbed and fluid phase. Isotherms can be constructed by solving equation 2 for the number of moles adsorbed, N_k, at any given combination of pressure and temperature.

$$\mu_{k,Fluid}(P,T) = \mu_{k,Adsorbed}(N_k,P,T) \quad (2)$$

The exact expressions for $\mu_{k,Fluid}(P,T)$ and $\mu_{k,Adsorbed}(N_k,P,T)$, as well as a number of other expressions can be found in the supporting information. For further details about the RALF model, we refer the reader to refs. [37,38]

Zero Length Column

The ZLC method is in essence a chromatographic technique, whereby the desorption of a previously equilibrated adsorbent is monitored. Equilibration occurs in a dilute mixture of adsorbate in inert (i.e. non-adsorbing) carrier, whereas desorption takes place in the pure inert carrier. The small amount of sample (< 15 mg) allows for neglecting external mass and heat transfer resistances and the short length of the column allows for treating the system as a well-mixed cell (CSTR), due to negligible axial concentration gradients[43]. Pressure drops are additionally assumed to be negligible and the system is treated as being isothermal.

The overall mass balance for the ZLC is well documented[32] and can also be found in the supporting information (eq. S8 and S9). Here we pay particular attention to the differential mass balance for the spherical adsorbent particle:

$$\frac{dq}{dt} = \frac{1}{r^2}\frac{\partial}{\partial r}(-r^2 J) \quad (3)$$

Where J is the flux, defined as:

$$J = -D_c(\bar{q})\ \frac{q}{RT}\frac{\partial \mu}{\partial r} = -D_c(\bar{q}) D^k \frac{\partial q}{\partial r} \quad (4)$$

Here, $D_c(\bar{q})$ is the corrected diffusivity and $D^k = \frac{q}{RT}\frac{\partial \mu_{CO2}}{\partial q}$ is the Darken correction factor, where $\frac{\mu_{CO_2}}{RT}$ is the reduced chemical potential of CO_2, as expressed in equation S5; the differential term $\frac{1}{RT}\frac{\partial \mu_{CO2}}{\partial q}$ can easily be obtained by appropriate derivation of this expression. The dependence of the corrected diffusivity on the average amount adsorbed, $\bar{q}$, is discussed in detail in the Results section. It is an important deviation from simpler kinetic models, which employ a constant diffusivity, and reflects the changing kinetics of an adsorbent undergoing structural changes.

The initial conditions are for the differential equations are:

$$c|_{t=0} = c_0 \quad (5)$$

$$q|_{r,t=0} = q_{RALF}(c_0) \quad (6)$$

With boundary conditions:

$$\left(\frac{dq}{dr}\right)_{r=0} = 0 \quad (7)$$

$$q|_{r=R} = q_{RALF}(c) \quad (8)$$

The subscript *RALF* in equations 6 and 8 indicates that the initial adsorbed phase concentration and the adsorbed phase concentration at the particle surface are in equilibrium with the gas phase, and so is known through our RALF equilibrium model. It should be noted that for a flexible material, the particle radius itself is a function of the adsorbed phase concentration. However, the breathing behaviour of the sample considered in this work is not dramatic, and so a constant average radius of the sample is assumed. This suits the purpose of this model, which is to describe the diffusivity behaviour of (Na,TEA)-ZSM-25 with a computationally fast and reliable set of equations.

The set of differential-algebraic equations have been solved numerically in MATLAB with the method of lines, using the function “ode15s”. The radial coordinate has been discretised with orthogonal collocation on finite elements.

Results

Structural characterisation

The structure of the *hydrated* as-prepared (Na,TEA)-ZSM-25 has been reported in detail by Guo et al.[27]. TEA^+ cations, which in combination with Na^+ direct the gel crystallisation to ZSM-25, were determined to occupy *pau* and *plg* cages. All of the RHO family of structures adopt the $Im\bar{3}m$

symmetry in the hydrated form, but upon dehydration the structures of Rho, PST-29 and ECR-18 have been observed to adopt $I\bar{4}3m$ symmetry as the structure distorts.

Here we focus on the *dehydrated* structures of both calcined and templated Na-ZSM-25. To determine the structure of the dehydrated samples of ZSM-25 from the powder diffraction data it was necessary to generate a starting structural model. To achieve this, the crystal structure of a pure SiO_2 form of ZSM-25 was modelled using the GULP program[44]. Starting from an energy minimised model for ZSM-25 in $Im\bar{3}m$ with a unit cell approaching the value observed for the hydrated form (45 Å), the symmetry was removed and the unit cell decreased stepwise to 43 Å. At each step the framework structure was energy minimised at constant volume in space group *P*1. Subsequently the closest symmetry of the modelled form was found to be $I\bar{4}3m$, and the structure was converted to this space group. The symmetry change from $Im\bar{3}m$ to $I\bar{4}3m$ results in an increase in the number of crystallographically distinct Si/Al sites from 16 to 30 and an increase in the number of O sites from 40 to 70, underlining the complexity of the structural refinement, and the need for strong T-O and O-O distance constraints.

The synchrotron data at 298 K as well as Rietveld refinements of the dehydrated materials are shown in the supporting information, Figures S3 – S5. A refinement summary and cation positions can also be found in the supporting information, Tables S1 – S3.

The structures of both dehydrated calcined and templated Na-ZSM-25 show significant reductions in unit cell parameter as compared to the reported hydrated structure, with values of 42.631(1), 42.980(1) and 45.0711(3) Å, respectively. The reduction in lattice parameters upon dehydration is due to the increased interaction of the Na^+ cations with the framework in the dehydrated structures. This results in distortions of the framework, with reduction in symmetry from $Im\bar{3}m$ (for the hydrated structure) to $I\bar{4}3m$. Both distorted frameworks and the relaxed, hydrated framework are shown in Figure 2, with a selection of computationally modelled structures for comparison. The slightly larger size of the templated material is due to the presence of bulky organic cations within the structure. Notably, the uptake on the as-prepared material is higher at pressures of 0-1 bar, despite the presence of template molecules, and this was chosen for the adsorption and modelling study.

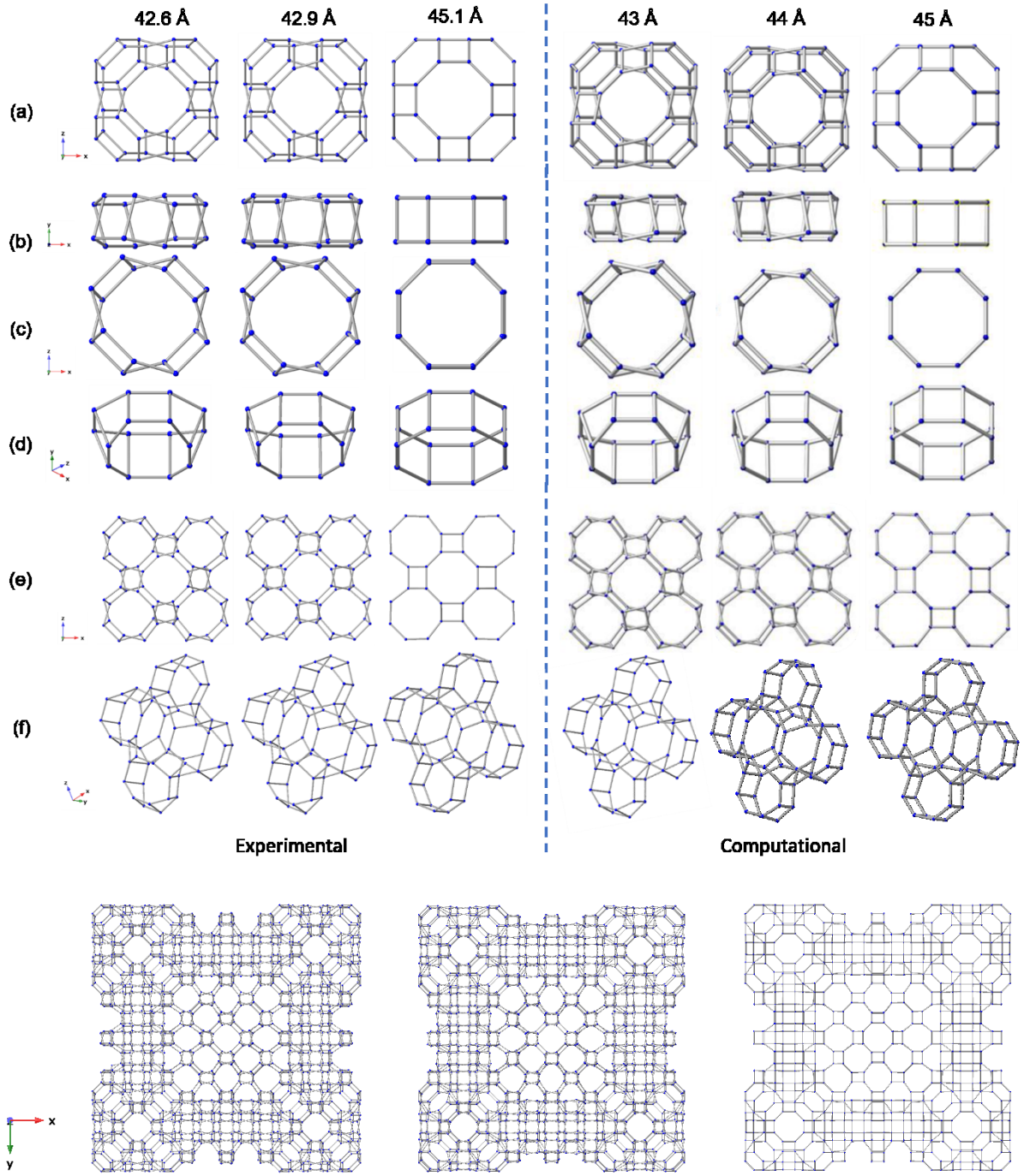

Figure 2: (Above) Structural units, from left to right of: dehydrated calcined; dehydrated as-prepared; hydrated as-prepared and computationally modelled ZSM-25, unit cell parameters displayed at the top. (a) lta *cages, (b,c,d)* d8r *units, (e,f)* pau *and adjacent* oto *cages. (Below) Extended frameworks of dehydrated Na,H-, dehydrated Na,TEA- and hydrated Na,TEA-ZSM-25 from left to right.*

Upon CO_2 exposure, unit cell expansion of (Na,TEA)-ZSM-25 takes place, similar to the effect of exposure to ambient moisture, as easily seen in Figures S6 and S7 in the supporting information, which show the synchrotron X-ray diffraction patterns for dehydrated and hydrated (Na,TEA)-ZSM-25 as well as a templated sample exposed to 860 mbar CO_2 at 298 K. Refinement of the structure of (Na,TEA)-ZSM-25 upon CO_2 adsorption was not possible due to the complex nature of the structure with CO_2 molecules in the structure. Analysis of peak positions, however, shows that upon adsorbing

CO_2 the sample exhibits unit cell parameters intermediate between those of the dehydrated and hydrated structures, of around 44 Å. We think that the framework adopts a structure similar to that predicted by computational methods for a cell with these dimensions. Although this predicted cell still shows framework distortions, the expansion is already leading to some significant framework relaxation. The evolution of lattice parameters with CO_2 adsorption was studied in more detail using variable pressure X-ray diffraction (VP-XRD). Due to the Mo X-ray source on the diffractometer used for this experiment and the lack of monochromation, the data are of insufficient quality to carry out Rietveld refinements and determine detailed structural properties, such as cation positions and cage and window distortions. Nevertheless, the data do show a strong relationship between the lattice volume and CO_2 partial pressure, as shown in Figure 3 (and Figure S8 in supporting information). A gradual expansion of the lattice parameters can be seen up to 43.55 Å, at which point a step occurs with rapid further expansion. The data at 328 K shows a more gradual expansion than those at 298 K, due to the smaller uptake of CO_2 at identical pressures. Despite the data between 0.20 and 0.60 bar suggesting a possibility of the presence of 2 phases of (Na,TEA)-ZSM-25 with very similar structures (both *I*-43*m* symmetry) and unit cell sizes, patterns were fitted as a single phase with one lattice parameter, as poor resolution makes unambiguous determination of a two phase system impossible. The unit cell parameters reach 44.49 Å at pCO_2 of 1 bar at 298 K.

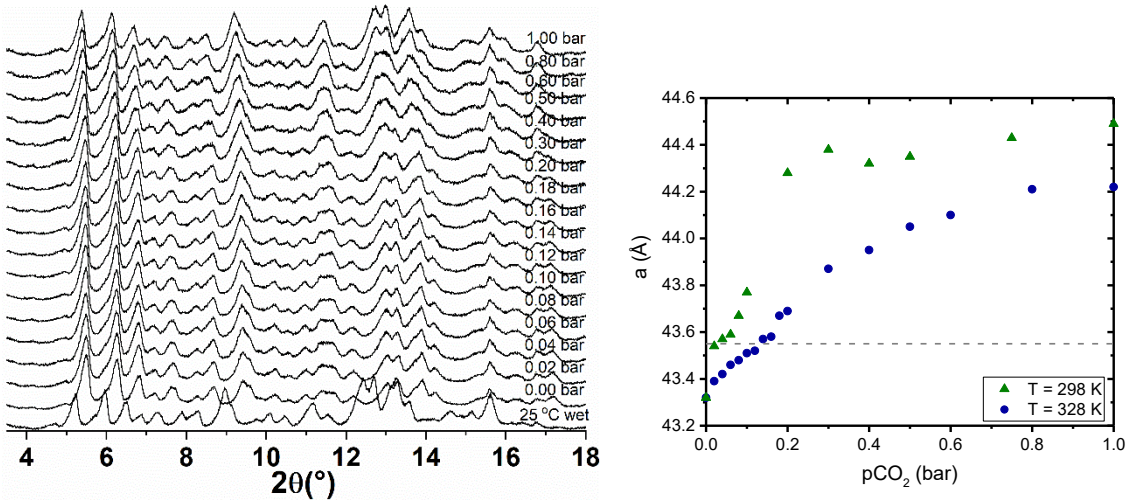

Figure 3: (Left) Variable pressure X-ray patterns for (Na,TEA)-ZSM-25 at different pCO_2 at 328 K (data set for hydrated structure also shown for comparison). (Right) Evolution of cubic lattice parameters as a function of CO_2 pressure at 298 K and 328 K. A step in the evolution is observed at constant lattice parameter of 43.55 Å.

Experimental CO_2 isotherms

CO_2 isotherms are shown in Figure 4, both in linear and logarithmic scales. They all exhibit the typical two step profile, which was also reported by Min et al.[28,29]. The desorption branches (see supporting information, Figure S9) overlap the adsorption ones well, so the material does not seem affected by significant hysteresis effects. From the semi-log plot is clear that all isotherms exhibit their inflection at approximately the same amount adsorbed, ca. 0.6 mol kg^{-1}. The fact that the inflection occurs at constant amount adsorbed, as opposed to constant pressure, is significant and implies that the change in adsorption behaviour is a function of the chemical potential of the solid, rather than that of the fluid phase. The heat of adsorption at zero loading, ΔH_0, can be estimated from the Henry's Law region of the isotherms and by applying equations 9 and 10; this yields $-\Delta H_0 = 39.6$ kJ mol^{-1}.

This is significantly lower than the isosteric heat of adsorption as reported by Min et al.[29] for templated (Na,TEA)-ZSM-25, but seems in line with heats found for other members of the RHO family[28].

$$\ln(K_P) = \frac{\Delta S_0}{R} - \frac{\Delta H_0}{RT} \quad (9)$$

$$\frac{d\ln(K_P)}{d(1/T)} = -\frac{\Delta H_0}{R} \quad (10)$$

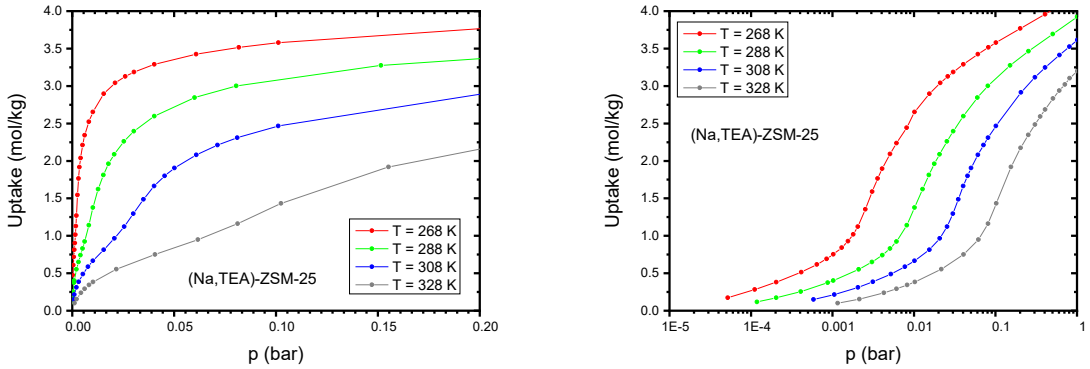

Figure 4: CO_2 isotherms for (Na,TEA)-ZSM-25 at various temperatures.

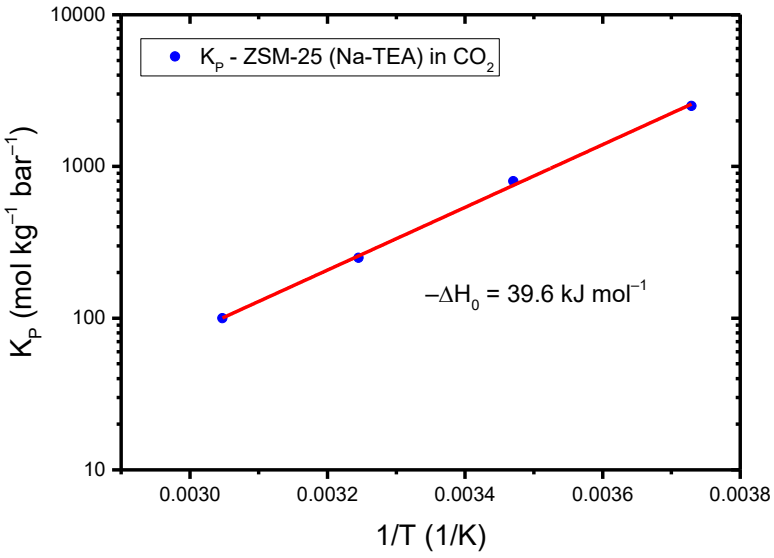

Figure 5: Henry's Law constants K_P for CO_2 adsorption on (Na,TEA)-ZSM-25 at different and calculated heat of adsorption at zero loading, ΔH_0.

Equilibrium model for (Na,TEA)-ZSM-25

RALF parameterisation for a single site solid

In order for the lattice fluid model to accurately describe the thermodynamics of the adsorbate – adsorbent system under consideration, it requires pure component characteristic parameters as outlined in ref.[37]. Consequently, through a set of mixing rules, these pure component parameters yield the characteristic parameters for the solid phase (itself a mixture of $(N_{ads}+1)$ components in the case of N_{ads} adsorbates; $N_{ads}=1$ in this work) at varying composition. The pure components are fully described by three characteristic parameters; here we choose to use the close-packed density, ρ^*, energy density, P^* and interaction energy, T^*. For several molecules, including CO_2, these parameters can be found in the literature; they have been listed in **Error! Reference source not found.**Table S7 in the supporting information.

The characteristic parameters for the solid can be obtained through a combination of physical characterisation techniques and isotherm fitting. The close-packed density, ρ_s^*, should correspond to the solid's skeletal density[37], which was measured by He pycnometry, i.e. $\rho_s^* = 2640$ kg m^{-3}. Similarly, the solid's energy density, P_s^* can be found through the heat of adsorption at zero loading by means of:

$$\Delta H_0 = \Delta U_0 + RT = \tilde{\rho}_s \frac{M_k}{\rho_k^*} 2P_{ks}^* \qquad 11$$

Where M_k is the molecular weight of the adsorbate and P_{ks}^* is the energy density for the solid – adsorbate pair, as defined by the mixing rule:

$$P_{ks}^* = (1-\kappa_{ks})\sqrt{P_s^* P_k^*} \qquad 12$$

Here, κ_{ks} is the binary interaction parameter, which is initially kept zero for parametrisation purposes. The reduced density of the solid , $\tilde{\rho}_s = \frac{\rho_s}{\rho_s^*}$, can be calculated using the actual density of the solid in vacuum; from our diffraction studies, ρ_s =2020 kg m^{-3}. The remaining parameters in equation 11 are pure component parameters for the adsorbate, i.e. CO_2, and are thus known. Substituting the various parameters yields $P_s^* = 1250$ MPa. It has to be noted that ideally, P_s^* should be determined using experimental or simulated heats of adsorption for a number of molecules, but since (Na,TEA)-ZSM-25 has not been studied extensively, we will suffice with the heat of adsorption for CO_2 alone. As the purpose of this work is to parametrise RALF in order to describe CO_2 isotherms specifically, this approach seems justified.

The final solid characteristic parameter, T_s^*, can initially be estimated from the Henry's Law constants[37], but is ultimately obtained by fitting to the experimental isotherms, as are κ_{ks} and the confinement parameter ξ_{kA}, which is defined as:

$$v_{kA}^* = \frac{v_k^*}{(1-\xi_{kA})} \qquad 13$$

Also,

$$\rho_{kA}^* = \rho_k^*(1-\xi_{kA}) \qquad 14$$

$$P_{kA}^{*} = P_{k}^{*}\left(1 - \xi_{kA}\right)$$

The introduction of ξ_{kA} acknowledges the fact that the adsorbed phase may not attain its bulk density in close-packing, due to geometric constrictions (or alternatively has an increased close-packed volume as compared to that of the bulk liquid, v_k^*). Equations 13-15 are alternative expressions to the ones reported in ref. [37], and constrain ξ_{kA} to values between 0 and 1.

The remaining input for the RALF model is the volumetric behaviour of (Na,TEA)-ZSM-25. Here we turn to the *in situ* VP-XRD measurements as presented in Figure 3. Rather than expressing the volumetric behaviour as a function of pCO_2, however, it would be more instructive to express it as a function of amount adsorbed. It is likely that structural changes occur once a critical amount of molecules have entered the zeolite's cages, triggering lattice expansion and/or cation movement. The fact that the steps in isotherms at different temperatures all occur at constant adsorbed phase concentration, are further indicative that this is indeed the case. Combining the isotherm data at 328 K with VP-XRD data, Figure 3 can be reconstructed to yield Figure 6.

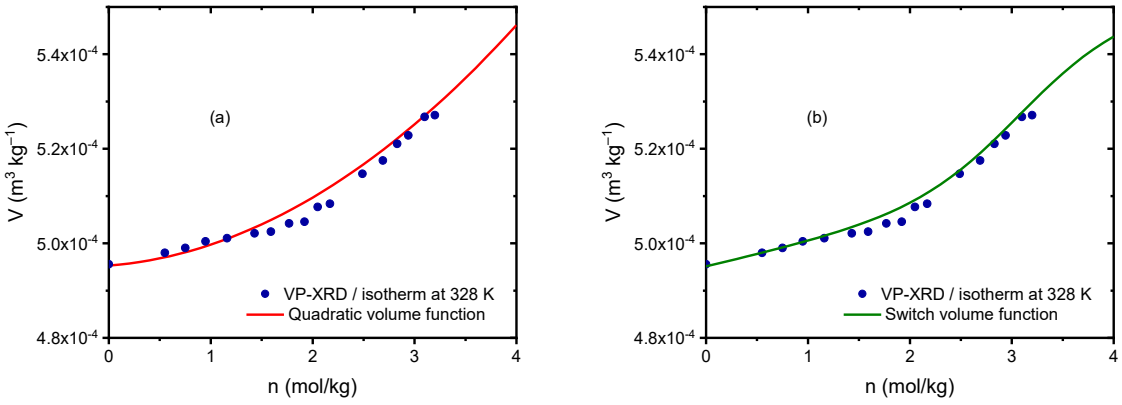

Figure 6: Specific volume vs. amount adsorbed. Blue dots are experimental data points from VP-XRD combined with isotherm data at 328 K. The experimental data have been modelled either using a quadratic function (a), or a switch function (b).

The smoothness of the steps in the isotherms and the lack of hysteresis suggest a different behaviour from the typical breathing transition in such materials as MIL-53 (Al), which could be modelled assuming two distinct solid phases which transition upon reaching critical stress levels (with concomitant hysteresis loops)[38]. Instead, here we will use continuous functions to describe any structural transitions in the adsorbent. As can be seen in Figure 6, two different functions were explored to describe the volumetric behaviour of (Na,TEA)-ZSM-25, namely a quadratic and so-called switch function. The expressions for these models and the corresponding model parameters can be found in the supporting information. When these volumetric model functions are used in a single site model and with the three remaining parameters, T_s^*, $\kappa_{CO2,s}$ and ξ_{CO2} used as fitting parameters, no satisfactory fits to the experimental isotherms could be obtained, as shown in Figures S10 and S11 in the supporting information (the values for the model parameters can be found in Table S7). Using the switch volume model results in a distinct step in the isotherms, but at the wrong partial CO_2 pressures (or amount adsorbed), whereas steps are completely absent in the case of using the quadratic function. In the case of the switch function, the inflection in the isotherms coincides with the inflection in the volume function, which occurs at an adsorbed concentration of approximately 3

mol kg^{-1}. Although the experimental VP-XRD data do show a marked increase in unit cell volume around this particular adsorbed phase concentration, the experimental isotherms do not show a corresponding step or inflection at this stage. This therefore suggests that the unit cell expansion is *not* the main cause of the observed steps in the experimental isotherms (which occur at the much lower concentration of 0.6 mol kg^{-1}). Taking these observations together, it seems highly unlikely that a single site model can capture the structural changes in (Na,TEA)-ZSM-25 that lead to the observed isotherm shape.

RALF parameterisation for a dual site solid

From the limited structural information that is available upon adsorption and based on behaviour of similar zeolite materials undergoing changes, we postulate the following dual site model to describe the equilibrium behaviour of (Na,TEA)-ZSM-25. It should be noted that this dual site model is conceptually different from the dual site Langmuir isotherms commonly used for typical zeolite isotherms (and used by Min et al. to fit each of the regions of the 2-step isotherm, i.e. above and below the step [28]). Our model comprises one site (or more accurately part of the total pore volume), α, which is always available for adsorption and a second site, β, which only becomes available upon reaching a certain adsorbed phase concentration in site α. The most likely physical mechanism behind this would be that cations are initially blocking the windows of the β-cages at low adsorbed phase concentration, preventing any molecules from being adsorbed. When CO_2 molecules start adsorbing onto the α-sites, the framework relaxation as a result of cation solvation is likely to afford movement of the blocking cations and upon reaching a threshold concentration this will allow CO_2 molecules to adsorb onto the β-sites. On desorption, the adsorbed molecules first leave the β-sites, before the cations move back to their original lattice positions. This prevents any CO_2 molecules from getting 'trapped' inside the β-site cages, as this would cause significant hysteresis effects, which is not observed experimentally. This postulated behaviour for (Na,TEA)-ZSM-25 is similar to the 'trapdoor' effect observed in closely related Na-Rho, where cations need to move through interaction with the adsorbate in order to allow significant adsorption to take place[16]. Although other mechanisms could also be responsible for the non-linear increase of pore volume with unit cell expansion, the dual site model is an empirical approach we use here to describe the observed sorption behaviour.

Since the α-site is always available for adsorption, it can be modelled like a regular site in RALF. In order to avoid any stray behaviour due to the volume changes in (Na,TEA)-ZSM-25, we opt to use the quadratic volume function described in the previous section, as it yields the correct isotherm behaviour at high pressures. The solid characteristic parameters listed in Table S7**Error! Reference source not found.** serve as a good starting point, leaving only the binary interaction parameters as adjustable parameters.

To model the behaviour of the β-site, we employ a strategy often used in molecular simulations. The site is effectively plugged at low adsorbed phase concentration, by giving it near zero porosity. The site porosity (or accessible pore volume) however is a function of the adsorbed amount on the α-site, in such a way that the β-site becomes available with increasing adsorbed phase concentration. The porosities of both sites eventually become identical at high adsorbed phase concentration or high pressure. Both sites also have identical solid characteristic parameters, but with different binary interaction parameters. Figure 7 shows how the porosity of both sites changes with amount adsorbed and how the two sites yield a composite isotherm, which closely resembles the experimentally observed ones. Figure 7b clearly shows how adsorption on the β-site starts when the adsorbed phase concentration reaches a value of around 0.6 mol kg^{-1}, which corresponds well with the inflection in the experimentally observed isotherms.

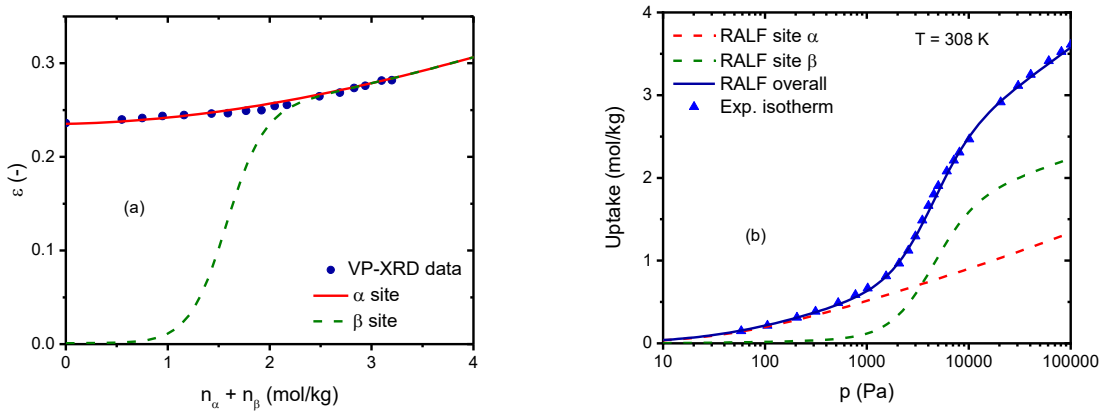

Figure 7: Porosity of both sites vs. amount adsorbed in both sites (a). Isotherms for two separate sites are added to yield the overall isotherm, matching experimental data (b).

The porosity function for the β-site in Figure 7a uses a switch function, which allows for the porosity to match that of the α-site near saturation. Expressed in terms of the site volume, it has the following form:

$$V_{s,\beta} = \left(1 - f(\bar{q})\right) \cdot \frac{1}{\rho_s^*} + f(\bar{q}) \cdot V_{s,\alpha}(\bar{q}) \qquad 16$$

where $V_{s,\alpha}$ is given by the quadratic function used in Figure 6a. $f(\bar{q})$ is a function of the form:

$$f(\bar{q}) = \frac{1}{2}(\tanh\{w \cdot (\bar{q} - \bar{q}_{trans})\} + 1) \qquad 17$$

where w and $\bar{q}_{trans}$ are adjustable parameters.

Using this approach results in good fits to the experimental isotherms at different temperatures, as shown in Figure 8a. The modelling parameters are listed Table 1. The dependency of the isosteric heat of adsorption with solid loading as obtained through the dual site RALF model can be seen in the Figure 8b and shows a sharp drop around the adsorbed phase concentration of 0.6 mol kg^{-1}, where the β-site starts adsorbing. Note that the heat of adsorption at zero loading is higher than obtained experimentally. This is a result from the non-zero value for the binary interaction parameter used for the α-site.

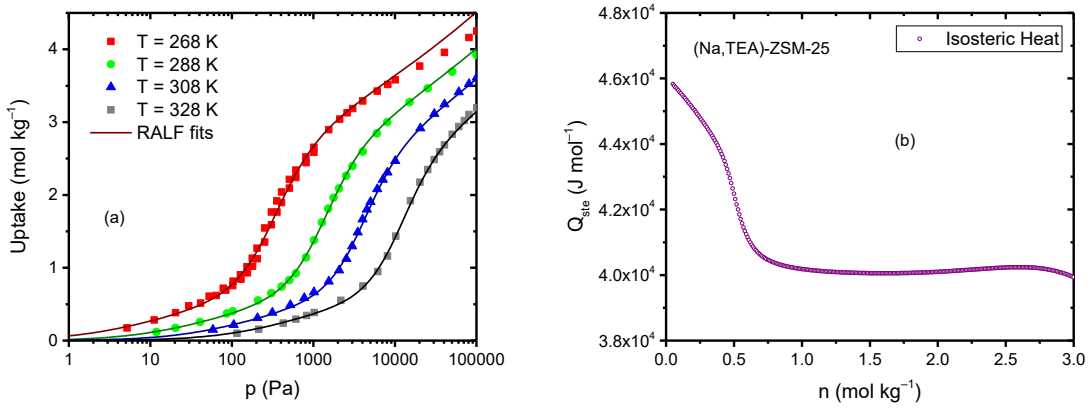

Figure 8: RALF dual site model and experimental isotherms at different temperatures (a). Isosteric heat of adsorption for ZSM-25 as obtained from dual site RALF model (b). A sharp drop of the heat is seen around the adsorbed phase concentration of 0.6 mol kg^{-1}.

Table 1: RALF dual site model parameters

	Site α	Site β
$\boldsymbol{P_s^*}$	1250	1250
$\boldsymbol{T_s^*}$	2050	2050
$\boldsymbol{\rho_s^*}$	2640	2640
$\kappa_{CO2,s}$	–0.085	–0.14
ξ_{CO2}	0.08	0.0
Site mass fraction	0.48	0.52
$\boldsymbol{w}$	n/a	2.75
$\overline{q}_{trans}$	n/a	1.62

Zero Length Column measurements

The results from the ZLC measurements at different flow rates at T = 308 K and adsorption in an atmosphere of pCO_2 = 0.2 bar, are shown in Figure 9 and Figure 10. The data shown were obtained by performing the mathematical procedure of deconvolution on the data as recorded by the mass spectrometer. This procedure removes extra-column effects, introduced by the experimental setup and is similar to a correction procedure reported in refs. [45,46], but takes into account diffusive elements within the setup. Therefore, the data shown here would correspond to the gas phase concentration leaving the ZLC, which incidentally is also what is simulated by the model equations, thus allowing for straightforward comparison between experiment and model. The original normalised signals can be found in the supporting information.

By integrating the area underneath the ZLC curves when shown in the $^{C}/_{C_0}$ vs. $F \times t$ (a so-called Ft plot, see Figure 10), CO_2 capacities can be obtained; these are listed in Table 2 and it can be seen that the ZLC method yields consistent results. The Ft plot is also useful visual tool in determining whether the desorption from the solid is an equilibrium process or if indeed it is governed by kinetic limitations. Equilibrium control, characterised by a flat, uniform concentration profile within the solid sphere is not affected by changing flow rates, and is thus evident from curves overlapping with each other; kinetic control on the other hand, where a significant adsorbed phase concentration profile exists, leads to curves diverging and is favoured at higher flow rates [32,47,48]. Figure 10 indicates

that the initial desorption, between $^{c}/_{c_0} = 1$ and the inflection at $^{c}/_{c_0} = 0.2$, is an equilibrium process under the measurement conditions, whereas at lower concentrations, that is, below the inflection, the Ft curves for different flow rates diverge, indicating kinetic control. Bearing in mind that the inflection in the ZLC response corresponds to the inflection in the isotherms and that the technique follows a desorption process, we can infer that under the measurement conditions presented here, CO_2 sorption is an equilibrium process when both α- and β-sites are accessible to the adsorbate, but becomes kinetically limited when the cations are moving back to the window positions, resulting in access to the β-sites being blocked.

Table 2: Calculated CO_2 capacity (based on wet mass of sample) for (Na,TEA)-ZSM-25 at different flow rates at 308 K

Flow rate ($cm^3\ min^{-1}$)	CO_2 capacity ($mol\ kg^{-1}$)
1	2.81
2	2.79
5	2.82
11	2.90
22	2.80

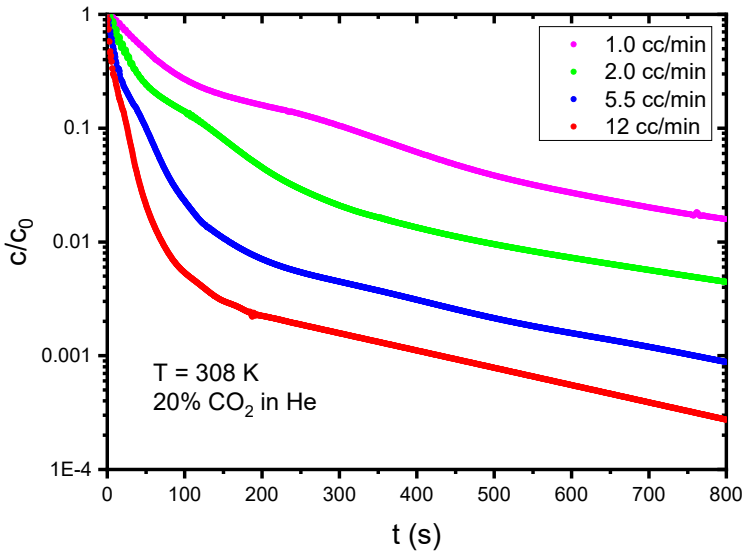

Figure 9: c/c0 vs time for (Na,TEA)-ZSM-25 at 308 K in pCO_2 = 0.2 bar

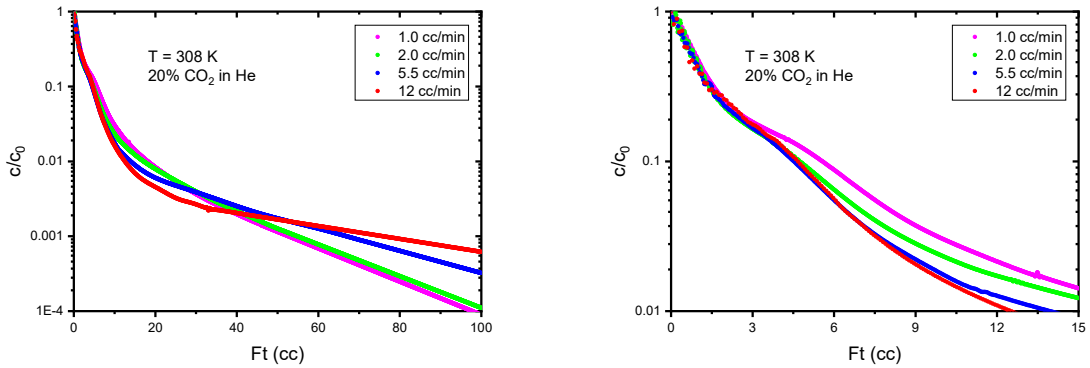

Figure 10: c/c0 vs. Ft for (Na,TEA)-ZSM-25 at 308 K in pCO_2 = 0.2 bar

At the low flow rate of 1 cm^3/min, the desorption of CO_2 is expected to be an equilibrium process throughout the entire concentration range and hence the simulated ZLC curves do not require fitting of kinetic parameters. The fit to the experimental data is shown in Figure 11, showing excellent agreement. Since the desorption under these conditions and at low partial pressures corresponds to the Henry's Law region of the isotherm, this data set can also be used to verify whether the Autosorb data had reached true equilibrium. Figure S13 in the supporting information shows that this is indeed the case.

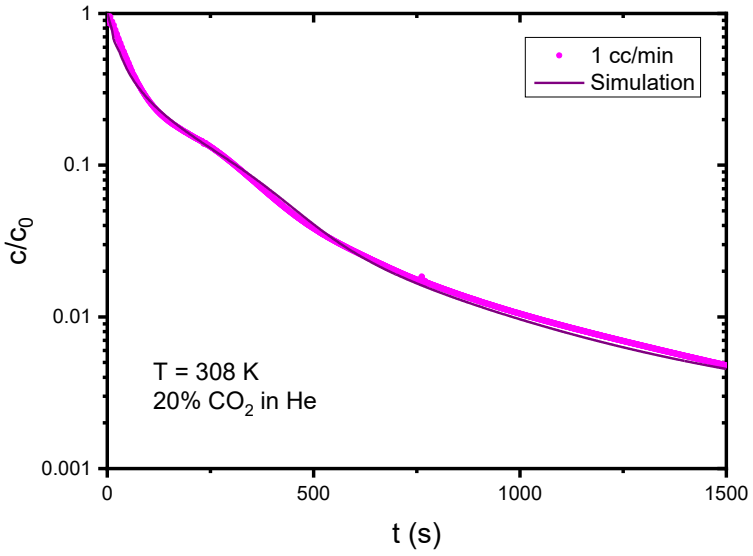

Figure 11: Deconvoluted experimental and simulated ZLC data at low flow rate of 1 cm^3/min, showing good agreement under equilibrium conditions.

Determination of kinetic parameters from ZLC measurements

To obtain information about the transport kinetics of CO_2 in (Na,TEA)-ZSM-25, we turn to the ZLC measurements at higher flow rates, where such limitations do arise. As discussed in the previous section, the CO_2 desorption in this material presents a particular case, which allows for a relatively straightforward way of analysing the data and obtain kinetic information. As the initial desorption

occurs under equilibrium conditions, whereby the adsorbed phase concentration profile remains uniform, this part of the desorption curve can simply be 'cut', leaving only the ZLC response for the desorption in the kinetically controlled concentration range. As shown in Figure 12, this cutting procedure removes the inflection and leaves a 'simple' curve which can now be modelled using a standard model for ZLC analysis and assuming some non-linearity, as presented in refs[32,34,35]. The gas phase concentration profile in this model is given by:

$$\frac{c(t)}{c_0} = \sum_{n=1}^{\infty} \frac{2L}{1 - \gamma\beta_n{}^2 - L - \beta_n{}^2 - \left(1 - L + \gamma\beta_n{}^2\right)^2} \times e^{-\beta_n{}^2 D_0 t/R^2} \quad 18$$

Here, L is the initial dimensionless flux at the surface of the solid at time zero, as determined by the isotherm's Henry's law constant, K, flowrate and diffusivity. It is defined as:

$$L = \frac{F}{3KV_s}\frac{R^2}{D} \quad 19$$

The ratio between solid and fluid phase accumulation is given by γ, which is usually low in gaseous systems:

$$\gamma = \frac{V_f}{3KV_s} \quad 20$$

Finally, β_n are the roots of the following equation:

$$\beta_n \cot \beta_n - 1 - \gamma\beta_n{}^2 + L = 0 \quad 21$$

The model fits to the 'cut' data (which have been re-normalised to give $\frac{c(t=0)}{c_0} = 1$) are also shown in Figure 12, providing a good match to the experimental data. The model parameters are listed in Table 3, with L_{app} and γ_{app} being apparent L and γ values, due to the non-linearity and the fact that the curves have been re-normalised. The fact that the standard model yields satisfactory fits to the experimental data, suggests that when desorption from (Na,TEA)-ZSM-25 becomes kinetically limited, the transport behaviour is more or less characterised by a single time constant.

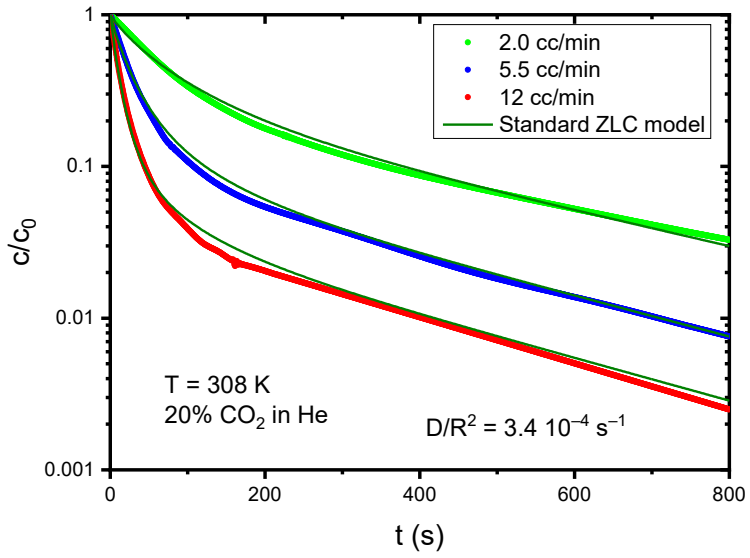

Figure 12: Analysis of 'cut' data using the standard ZLC model assuming a linear isotherm (equation 18) obtaining a single value for the diffusivity at low concentration range, i.e. $D/R^2 = 3.4 \times 10^{-4} s^{-1}$.

Table 3: Model parameters for the standard ZLC model fits to 'cut' and renormalized (Na,TEA)-ZSM-25 data at 308 K

Flow rate (cm^3/min)	L_{app}	γ_{app}	D/R^2 (s^{-1})
2.0	10	0.18	3.4×10^{-4}
5.5	26	0.18	3.4×10^{-4}
12	57	0.18	3.4×10^{-4}

Full curve fits using RALF equilibrium model

Rather than using the relationship based on a linear isotherm (equation 18), the aim of this study is to show how an alternative equilibrium model, i.e. the RALF model, can be used to obtain kinetic information. To this end, we must now find a kinetic model, which effectively describes how the CO_2 diffusivity evolves during the ZLC measurements. The kinetic results presented so far have shown that CO_2 transport is very rapid when both α- and β-sites are accessible, leading to desorption being an equilibrium process under the measurement conditions, whereas the diffusivity attains a rather constant limiting value when only the α-site is available for adsorption/desorption (see Figure 12). It is clear that the availability of the β-site and the transport properties are closely related and that they are likely associated with the unit cell decreasing with decreasing CO_2 concentration, but with the limited amount of structural information, we can only speculate as to what underpins this behaviour.

We are therefore proposing a mechanism whereby the diffusivity is controlled by repulsive forces between the CO_2 molecules and the zeolite framework. We know from the synchrotron results that at low CO_2 partial pressures, (Na,TEA)-ZSM-25 assumes a distorted cubic structure, with small lattice parameters. Upon adsorption, the interaction of the Na^+ cations with the framework reduces due to solvation by adsorbate molecules, causing the framework to relax towards a high symmetry structure with larger unit cell parameters. Although the unit cell effect is small at low adsorbed

phase concentration, small changes in window size could have large consequences for a material's transport behaviour. After all, these are likely to be controlled by repulsive forces, which will rapidly increase upon a decreasing distance between molecule and framework. A common way of describing the interaction between molecules in molecular simulations is through the Buckingham potential, where the repulsive term is of an exponential form[49,50]. Assuming that the diffusivity is inversely related to these repulsive forces and using the adsorbed phase concentration as a proxy for the intermolecular distance, we are proposing the following relationship:

$$D = D_0 + A \cdot e^{B(\bar{q}-\bar{q}_{trans})} \qquad 22$$

Here we recognise the fact that the diffusivity approaches a limiting value at low concentration, D_0, and that it rapidly increases upon reaching a critical adsorbed phase concentration, $\bar{q}_{trans}$, which can be estimated from the Ft plot, Figure 10. This leaves two modelling parameters, A and B, to be fitted to the experimental data.

Applying this kinetic model to the overall ZLC model yields good fits to the experimental data as shown in Figure 13. Here we have used the kinetic model parameters as listed in Table 4; $\bar{q}_{trans}$ coincides with the adsorbed phase concentration at which the step in the isotherms occur, i.e. $\bar{q}_{trans} = 0.6\ mol\ kg^{-1}$. As expected, D_0/R^2 is identical to the value found by applying the standard ZLC model to the 'cut' data. The kinetic analysis of ZLC data obtained at 288 K (to be found in the supporting information) was carried out in a similar fashion and, apart from a different value for D_0/R^2, uses identical modelling parameters, which serves as a validation of the model. The activation energy for diffusion at low concentration is estimated to be 23 – 34 kJ mol^{-1}; this large range is due to some uncertainties in a third data set, but nonetheless suggest the activation energy to be 0.6 – 0.9 times the heat of adsorption.

The evolution of diffusivity with adsorbed phase concentration can be found in Figure 14a. The transition into equilibrium control above $\bar{q}_{trans}$ is further aided by the Darken correction factor, $D^k = \frac{q}{RT}\frac{\partial \mu_{CO2}}{\partial q}$, as described in equation 4. As shown in Figure 14b, it is significantly larger than unity at the initial stages of desorption, leading to even faster transport kinetics.

Table 4: Kinetic model parameters used to fit full ZLC curves at 308 K

Kinetic model parameter	Value	
D_0/R^2	3.4×10^{-4}	s^{-1}
$\bar{q}_{\tau,trans}$	0.6	mol kg^{-1}
A	3.6×10^{-4}	s^{-1}
B	8.3	-

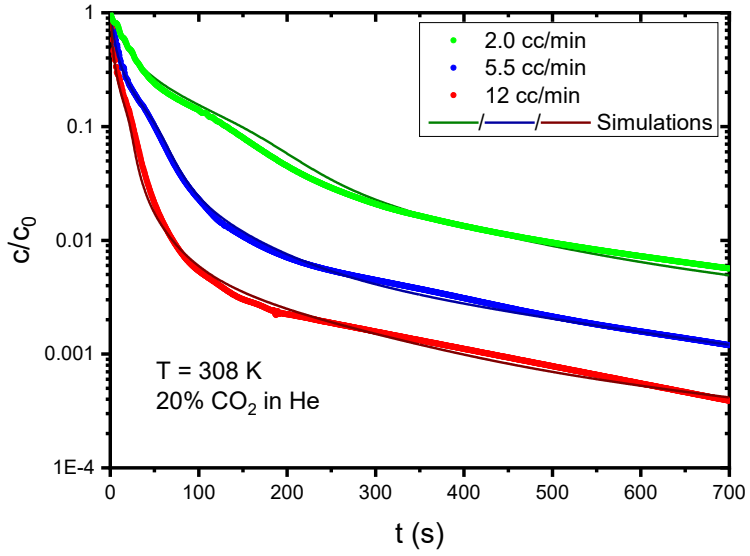

Figure 13: Deconvoluted experimental and simulated ZLC data using RALF model at higher flow rates, showing good agreement using the kinetic model in equation 22 with the parameters in Table 4.

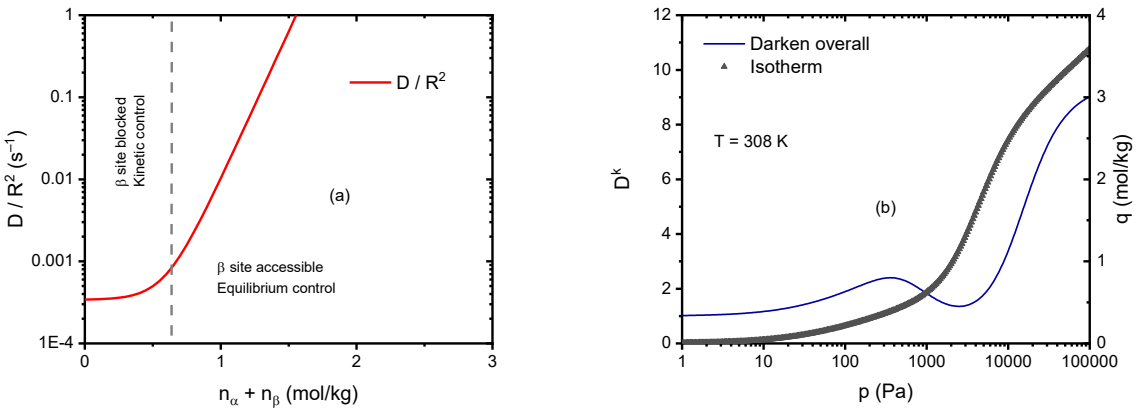

Figure 14: Evolution of diffusivity with adsorbed phase concentration according to equation 22 (a). Overall darken correction factor and isotherm at 308 K (b).

Discussion

The structural and physical properties of flexible zeolites are complex and difficult to study. This is particularly true for (Na,TEA)-ZSM-25 because of its structural and crystallographic complexity - the high number of crystallographically-distinct framework atoms and the partial occupancies of inorganic and organic extra-framework cations. This is complicated further upon adsorption of disordered CO_2 molecules, which can cause cation motion and themselves give rise to scattering. A detailed structural understanding is currently only available for two physical conditions, the fully dehydrated and hydrated ones, where hydration leads to a relaxation of the framework, due to a solvating effect of the water molecules with the Na ions. The effect of CO_2 adsorption is expected to be intermediate on this adsorption-induced spectrum, but further studies would be required to fully understand which intermediate structural transitions may occur, particularly around the inflection

point in the isotherm. Here, we can only speculate on the type of adsorption-induced mechanism which could explain the equilibrium and kinetic behaviour observed in this work, with reference to literature evidence.

Our equilibrium model employs a dual site isotherm, assuming that one site is blocked at low partial pressures. The relative capacities of the α- and β- regions of the micropore volume (ca. 1:2) indicate that these regions must contain one or more of the most abundant cages in the structure (the *oto*, *gsm* and *phi* cages are the most abundant – see Figure 1 for details).

Examination of window sizes in dehydrated (Na,TEA)-ZSM-25 as determined by the shortest O – O distance across the centre of 8Rs (corrected for the van der Waals radii of two O atoms), shown in Figure 15, suggests that no windows are sufficiently small to limit percolation of CO_2 through the structure, or make particular assemblies of cavities inaccessible at low partial pressure. Despite the kinetic diameter of a CO_2 molecule being 2.98 Å[51], it was shown to cross windows with a crystallographic free dimension of 1.9 Å in Li-RHO[24]. Additionally, the high connectivity of cavities in ZSM-25 makes it unlikely that any one area within the unit cell is completely blocked off from CO_2 molecules. We have therefore postulated that access to the β-sites is instead controlled by the presence of blocking organic and inorganic cations. As CO_2 adsorbs onto the accessible site, the framework relaxation will cause the blocking cations to move, thus making the β-sites available at higher pressures. Although the exact structural mechanisms for the adsorption behaviour described here is not yet understood it is clear that the presence and nature of the cations is crucial to this behaviour.

It is interesting to note that exhaustive ion exchange to other cation forms greatly alters the adsorption behaviour of ZSM-25. Both (Li,TEA)- and (K,TEA)-ZSM-25 exhibit typical Type I adsorption behaviour, but with approximately half the uptake of the (Na,TEA)-form at a CO_2 partial pressure of 1 bar, as shown in Figure S18. The behaviour of these materials shows that the step observed in the adsorption isotherm is a cation mediated process and that Li and K cations inhibit this stepped behaviour. Similar results have been reported by Min et al.[28], which suggest that in fact only the Na and Cs cation forms induce a step in the isotherm at pressures below 1 bar. Similar effects on adsorption behaviour have also been observed in other frameworks, where structural changes seem to be delicately balanced by the size of different cations[23].

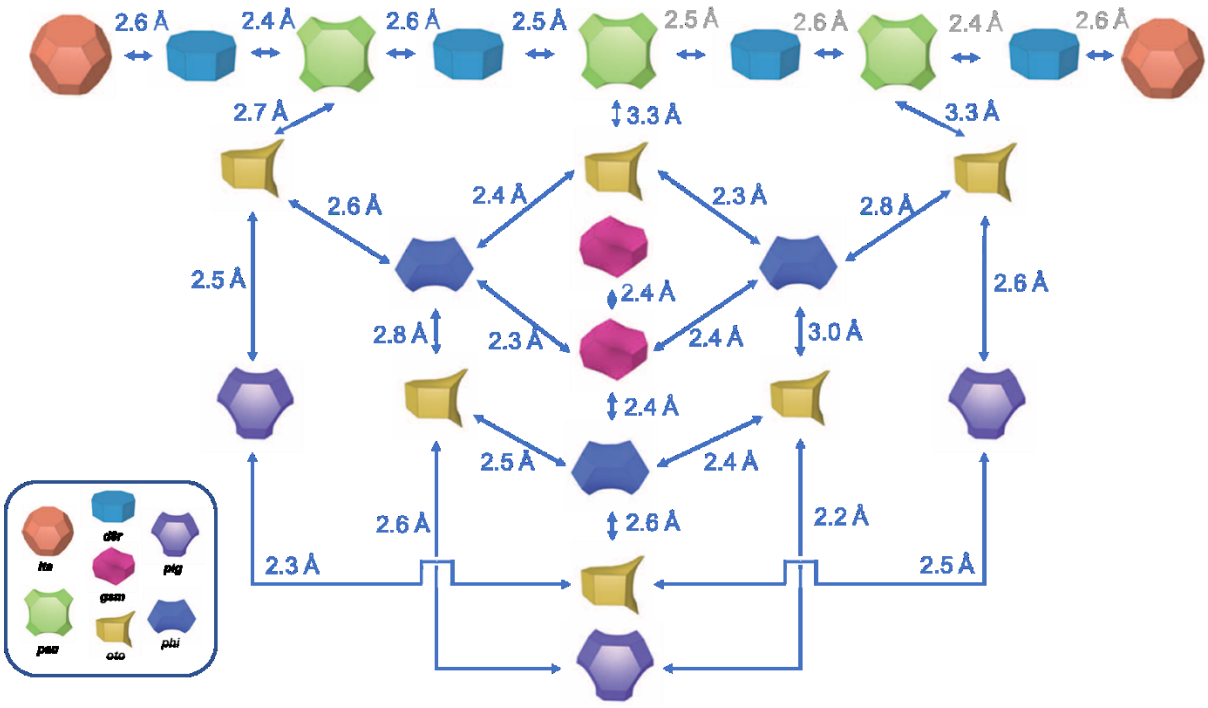

Figure 15: Window sizes between cavities present in dehydrated (Na,TEA)-ZSM-25. Greyed out numbers indicate symmetry related to an already shown window size.

Our kinetic model employs repulsive interactions as the mechanism for diffusivity behaviour with changing adsorbed phase concentration. Table 5 provides a selection of window sizes in both the dehydrated and hydrated structures, showing a dramatic increase of up to 65% for most of these (a full list is available in the supporting information, Table S9). We observe the structure to expand with adsorbed CO_2, increasing with uptake to be ca. 44.5 Å at 1 bar at 298 K, and it seems that the clear inflection in the adsorption isotherm corresponds to a change in the structure that is important for CO_2 uptake into the β-site.

Table 5: Selected window sizes in dehydrated and hydrated structures of (Na,TEA)-ZSM-25

Cages connected by window	Dehydrated window size (Å)	Hydrated window size (Å)
lta – d8r	2.6	3.8
d8r – pau	2.4	3.9
pau – oto	3.3	3.1
oto – phi	2.4	3.8
phi – gsm	2.3	3.4
oto – plg	2.5	3.8

Since repulsion and interatomic distance are strongly related, our current kinetic model seems justified. However, we have also considered an alternative mechanism for the kinetic behaviour, whereby the transition from kinetic to equilibrium control is governed by the (un)-availability of the β-site. As discussed previously, the two interpenetrating networks of interconnected channels in

(Na,TEA)-ZSM-25 lead to a high degree of connectivity of the cavities. This may lead to a situation where access of a molecule to one cavity may be through a set of other cavities. In the case of cations blocking access to certain cages, access to other cages may therefore become kinetically hindered, as the molecule effectively has to find an alternative, longer, route to the adsorption site. To explain our experimentally observed results, however, such a mechanism would require that the diffusive path of the molecule increases by a factor of ~10, which seems implausible. Our current interpretation based on window distortion leading to increased repulsive interaction makes more physical sense, but more importantly, is compatible with our data from kinetic experiments.

It is finally worth noting that our kinetic studies indicate a significant difference in transport behaviour on either side of the step in the isotherm, which seem to contradict findings by Min et al. [28]. Our study provides a more detailed exploration of the pre-step ($n < 0.6\ mol\ kg^{-1}$) kinetics however, and it is done at temperatures which are more likely to emphasise these features. Overall, despite some kinetic limitations at low concentration, CO_2 sorption in (Na,TEA)-ZSM-25 is significantly faster than in closely related Na-Rho, whilst uptake is still considerable.

Conclusions

We have described a methodology to elucidate the equilibrium and kinetic adsorption behaviour of flexible zeolites by using a combination of characterisation and modelling techniques. The structural behaviour of (Na,TEA)-ZSM-25, a member of the extended RHO-family of zeolites, in the presence of CO_2 proved to be too complex to solve through standard refinement techniques. A detailed understanding of the fully distorted (dehydrated) and fully relaxed (hydrated) frameworks was however obtained through refinement of synchrotron X-ray diffraction, and shows significant cell as well as window size expansion upon hydration. Variable pressure X-ray pressure corroborates this behaviour in the presence of CO_2, although full relaxation of the framework cannot be attained at CO_2 pressures of 1 bar and below.

Lattice fluid modelling, conversely, suggests that cell expansion cannot directly be the main driver of the characteristic two step adsorption behaviour (as it is, for example in the MOF MIL-53). Partial site inaccessibility on the other hand, tentatively attributed to window blocking cations, can be used to great effect in our lattice fluid model to accurately describe the experimentally observed isotherms.

Kinetic experiments of CO_2 desorption from (Na,TEA)-ZSM-25 show a rapidly evolving diffusivity with adsorbed phase concentration. Using our structural understanding of the dehydrated and hydrated structures, we have inferred a kinetic model based on repulsive forces exerted by cavity windows that CO_2 molecules have to cross in order to access their adsorption sites. Due to the exponential nature of the repulsive term in the Buckingham potential, even a modest change in unit cell parameters will lead to a drastic drop in repulsive forces and thus increase in diffusivity.

In summary, despite the complex nature of the structural, physical and kinetic behaviour of (Na,TEA)-ZSM-25 in the presence of CO_2, we have shown that by combining various experimental techniques we have arrived at a plausible mechanism for CO_2 adsorption and transport in flexible (Na,TEA)-ZSM-25. To our knowledge, this is also the first study to combine an equilibrium model that can capture adsorption induced framework flexibility with a kinetic analysis, allowing for changing kinetics as adsorption/desorption proceeds.

Acknowledgements

The authors thank the EPSRC for funding ('Cation-controlled gating for selective gas adsorption over adaptable zeolites': EP/N032942/1, VMG, PAW; EP/N033329/1, MV and SB; an NPIF PhD scholarship for ELB, EP/R512199/1). They also acknowledge assistance from Professor Andrew N. Fitch at beamline ID31 at the ESRF, Grenoble, and Dr. Stephen P. Thompson at beamline I11, Diamond Light Source, Harwell.

References

(1) Gaffney, T. R. Porous Solids for Air Separation. *Curr. Opin. Solid State Mater. Sci.* **1996**, *1* (1), 69–75. https://doi.org/10.1016/S1359-0286(96)80013-1.

(2) Rege, S. U.; Yang, R. T. Limits for Air Separation by Adsorption with LiX Zeolite. *Ind. Eng. Chem. Res.* **1997**, *36* (12), 5358–5365. https://doi.org/10.1021/ie9705214.

(3) Delgado, J. A.; Águeda, V. I.; Uguina, M. A.; Sotelo, J. L.; Brea, P.; Grande, C. A. Adsorption and Diffusion of H2, CO, CH4, and CO2 in BPL Activated Carbon and 13X Zeolite: Evaluation of Performance in Pressure Swing Adsorption Hydrogen Purification by Simulation. *Ind. Eng. Chem. Res.* **2014**, *53* (40), 15414–15426. https://doi.org/10.1021/ie403744u.

(4) Palomino, M.; Corma, A.; Rey, F.; Valencia, S. New Insights on CO2−Methane Separation Using LTA Zeolites with Different Si/Al Ratios and a First Comparison with MOFs. *Langmuir* **2010**, *26* (3), 1910–1917. https://doi.org/10.1021/la9026656.

(5) Moliner, M.; Martínez, C.; Corma, A. Synthesis Strategies for Preparing Useful Small Pore Zeolites and Zeotypes for Gas Separations and Catalysis. *Chem. Mater.* **2014**, *26* (1), 246–258. https://doi.org/10.1021/cm4015095.

(6) Cheung, O.; Hedin, N. Zeolites and Related Sorbents with Narrow Pores for CO2 Separation from Flue Gas. *RSC Adv.* **2014**, *4* (28), 14480–14494. https://doi.org/10.1039/C3RA48052F.

(7) Cheung, O.; Bacsik, Z.; Krokidas, P.; Mace, A.; Laaksonen, A.; Hedin, N. K+ Exchanged Zeolite ZK-4 as a Highly Selective Sorbent for CO2. *Langmuir* **2014**, *30* (32), 9682–9690. https://doi.org/10.1021/la502897p.

(8) Palomino, M.; Corma, A.; Jordá, J. L.; Rey, F.; Valencia, S. Zeolite Rho: A Highly Selective Adsorbent for CO2/CH4 Separation Induced by a Structural Phase Modification. *Chem. Commun.* **2012**, *48* (2), 215–217. https://doi.org/10.1039/C1CC16320E.

(9) Shang, J.; Hanif, A.; Li, G.; Xiao, G.; Liu, J. Z.; Xiao, P.; Webley, P. A. Separation of CO2 and CH4 by Pressure Swing Adsorption Using a Molecular Trapdoor Chabazite Adsorbent for Natural Gas Purification. *Ind. Eng. Chem. Res.* **2020**, *59* (16), 7857–7865. https://doi.org/10.1021/acs.iecr.0c00317.

(10) Liu, Q.; Pham, T.; Porosoff, M. D.; Lobo, R. F. ZK-5: A CO2-Selective Zeolite with High Working Capacity at Ambient Temperature and Pressure. *ChemSusChem* **2012**, *5* (11), 2237–2242. https://doi.org/10.1002/cssc.201200339.

(11) Fyfe, C. A.; Kennedy, Gordon. J.; De Schutter, C. T.; Kokotailo, G. T. Sorbate-Induced Structural Changes in ZSM-5 (Silicalite). *J. Chem. Soc. Chem. Commun.* **1984**, No. 8, 541–542. https://doi.org/10.1039/C39840000541.

(12) Tezel, O. H.; Ruthven, D. M. Sorption of Benzene in NaX Zeolite: An Unusual Hysteresis Effect. *J. Colloid Interface Sci.* **1990**, *139* (2), 581–583. https://doi.org/10.1016/0021-9797(90)90132-8.

(13) Kärger, J.; Binder, T.; Chmelik, C.; Hibbe, F.; Krautscheid, H.; Krishna, R.; Weitkamp, J. Microimaging of Transient Guest Profiles to Monitor Mass Transfer in Nanoporous Materials. *Nat. Mater.* **2014**, *13* (4), 333–343. https://doi.org/10.1038/nmat3917.

(14) Jeffroy, M.; Fuchs, A. H.; Boutin, A. Structural Changes in Nanoporous Solids Due to Fluid Adsorption: Thermodynamic Analysis and Monte Carlo Simulations. *Chem. Commun.* **2008**, No. 28, 3275–3277. https://doi.org/10.1039/B805117H.

(15) Coudert, F.-X.; Jeffroy, M.; Fuchs, A. H.; Boutin, A.; Mellot-Draznieks, C. Thermodynamics of Guest-Induced Structural Transitions in Hybrid Organic−Inorganic Frameworks. *J. Am. Chem. Soc.* **2008**, *130* (43), 14294–14302. https://doi.org/10.1021/ja805129c.

(16) Lozinska, M. M.; Mangano, E.; Mowat, J. P. S.; Shepherd, A. M.; Howe, R. F.; Thompson, S. P.; Parker, J. E.; Brandani, S.; Wright, P. A. Understanding Carbon Dioxide Adsorption on Univalent Cation Forms of the Flexible Zeolite Rho at Conditions Relevant to Carbon Capture from Flue Gases. *J. Am. Chem. Soc.* **2012**, *134* (42), 17628–17642. https://doi.org/10.1021/ja3070864.

(17) Remy, T.; Baron, G. V.; Denayer, J. F. M. Modeling the Effect of Structural Changes during Dynamic Separation Processes on MOFs. *Langmuir* **2011**, *27* (21), 13064–13071. https://doi.org/10.1021/la203374a.

(18) Schneemann, A.; Bon, V.; Schwedler, I.; Senkovska, I.; Kaskel, S.; Fischer, R. A. Flexible Metal–Organic Frameworks. *Chem. Soc. Rev.* **2014**, *43* (16), 6062–6096. https://doi.org/10.1039/C4CS00101J.

(19) Greenaway Alex G.; Shin Jiho; Cox Paul A.; Shiko Elenica; Thompson Stephen P.; Brandani Stefano; Hong Suk Bong; Wright Paul A. Structural Changes of Synthetic Paulingite (Na,H-ECR-18) upon Dehydration and CO2 Adsorption. *Z. Für Krist. - Cryst. Mater.* **2015**, *230* (4), 223. https://doi.org/10.1515/zkri-2014-1824.

(20) Choi, H. J.; Min, J. G.; Ahn, S. H.; Shin, J.; Hong, S. B.; Radhakrishnan, S.; Chandran, C. V.; Bell, R. G.; Breynaert, E.; Kirschhock, C. E. A. Framework Flexibility-Driven CO2 Adsorption on a Zeolite. *Mater. Horiz.* **2020**, *7* (6), 1528–1532. https://doi.org/10.1039/D0MH00307G.

(21) Shang, J.; Li, G.; Singh, R.; Gu, Q.; Nairn, K. M.; Bastow, T. J.; Medhekar, N.; Doherty, C. M.; Hill, A. J.; Liu, J. Z.; Webley, P. A. Discriminative Separation of Gases by a "Molecular Trapdoor" Mechanism in Chabazite Zeolites. *J. Am. Chem. Soc.* **2012**, *134* (46), 19246–19253. https://doi.org/10.1021/ja309274y.

(22) Serre, C.; Millange, F.; Thouvenot, C.; Noguès, M.; Marsolier, G.; Louër, D.; Férey, G. Very Large Breathing Effect in the First Nanoporous Chromium(III)-Based Solids: MIL-53 or CrIII(OH)·{O2C−C6H4−CO2}·{HO2C−C6H4−CO2H}x·H2Oy. *J. Am. Chem. Soc.* **2002**, *124* (45), 13519–13526. https://doi.org/10.1021/ja0276974.

(23) Georgieva, V. M.; Bruce, E. L.; Verbraeken, M. C.; Scott, A. R.; Casteel, W. J.; Brandani, S.; Wright, P. A. Triggered Gate Opening and Breathing Effects during Selective CO2 Adsorption by Merlinoite Zeolite. *J. Am. Chem. Soc.* **2019**, *141* (32), 12744–12759. https://doi.org/10.1021/jacs.9b05539.

(24) Lozinska, M. M.; Mangano, E.; Greenaway, A. G.; Fletcher, R.; Thompson, S. P.; Murray, C. A.; Brandani, S.; Wright, P. A. Cation Control of Molecular Sieving by Flexible Li-Containing Zeolite Rho. *J. Phys. Chem. C* **2016**, *120* (35), 19652–19662. https://doi.org/10.1021/acs.jpcc.6b04837.

(25) Van Assche, T. R. C.; Baron, G. V.; Denayer, J. F. M. Molecular Separations with Breathing Metal–Organic Frameworks: Modelling Packed Bed Adsorbers. *Dalton Trans.* **2016**, *45* (10), 4416–4430. https://doi.org/10.1039/C6DT00258G.

(26) Serre C.; Bourrelly S.; Vimont A.; Ramsahye N. A.; Maurin G.; Llewellyn P. L.; Daturi M.; Filinchuk Y.; Leynaud O.; Barnes P.; Férey G. An Explanation for the Very Large Breathing Effect of a Metal–Organic Framework during CO2 Adsorption. *Adv. Mater.* **2007**, *19* (17), 2246–2251. https://doi.org/10.1002/adma.200602645.

(27) Guo, P.; Shin, J.; Greenaway, A. G.; Min, J. G.; Su, J.; Choi, H. J.; Liu, L.; Cox, P. A.; Hong, S. B.; Wright, P. A.; Zou, X. A Zeolite Family with Expanding Structural Complexity and Embedded Isoreticular Structures. *Nature* **2015**, *524*, 74.

(28) Min, J. G.; Kemp, K. C.; Lee, H.; Hong, S. B. CO2 Adsorption in the RHO Family of Embedded Isoreticular Zeolites. *J. Phys. Chem. C* **2018**, *122* (50), 28815–28824. https://doi.org/10.1021/acs.jpcc.8b09996.

(29) Min, J. G.; Kemp, K. C.; Hong, S. B. Zeolites ZSM-25 and PST-20: Selective Carbon Dioxide Adsorbents at High Pressures. *J. Phys. Chem. C* **2017**, *121* (6), 3404–3409. https://doi.org/10.1021/acs.jpcc.6b11582.
(30) Zhao, J.; Xie, K.; Singh, R.; Xiao, G.; Gu, Q.; Zhao, Q.; Li, G.; Xiao, P.; Webley, P. A. Li+/ZSM-25 Zeolite as a CO2 Capture Adsorbent with High Selectivity and Improved Adsorption Kinetics, Showing CO2-Induced Framework Expansion. *J. Phys. Chem. C* **2018**, *122* (33), 18933–18941. https://doi.org/10.1021/acs.jpcc.8b04152.
(31) Eic, M.; Ruthven, D. M. A New Experimental Technique for Measurement of Intracrystalline Diffusivity. *Zeolites* **1988**, *8* (1), 40–45. https://doi.org/10.1016/S0144-2449(88)80028-9.
(32) Brandani, S.; Ruthven, D. M. Analysis of ZLC Desorption Curves for Gaseous Systems. *Adsorption* **1996**, *2* (2), 133–143. https://doi.org/10.1007/BF00127043.
(33) Hu, X.; Mangano, E.; Friedrich, D.; Ahn, H.; Brandani, S. Diffusion Mechanism of CO2 in 13X Zeolite Beads. *Adsorption* **2014**, *20* (1), 121–135. https://doi.org/10.1007/s10450-013-9554-z.
(34) Brandani, S.; Jama, M. A.; Ruthven, D. M. ZLC Measurements under Non-Linear Conditions. *Chem. Eng. Sci.* **2000**, *55* (7), 1205–1212. https://doi.org/10.1016/S0009-2509(99)00411-X.
(35) Brandani, S. Effects of Nonlinear Equilibrium on Zero Length Column Experiments. *Chem. Eng. Sci.* **1998**, *53* (15), 2791–2798. https://doi.org/10.1016/S0009-2509(98)00075-X.
(36) Friedrich, D.; Mangano, E.; Brandani, S. Automatic Estimation of Kinetic and Isotherm Parameters from ZLC Experiments. *Chem. Eng. Sci.* **2015**, *126*, 616–624. https://doi.org/10.1016/j.ces.2014.12.062.
(37) Brandani, S. The Rigid Adsorbent Lattice Fluid Model for Pure and Mixed Gas Adsorption. *AIChE J.* **2019**, *65* (4), 1304–1314. https://doi.org/10.1002/aic.16504.
(38) Verbraeken, M. C.; Brandani, S. Predictions of Stepped Isotherms in Breathing Adsorbents by the Rigid Adsorbent Lattice Fluid. *J. Phys. Chem. C* **2019**, *123* (23), 14517–14529. https://doi.org/10.1021/acs.jpcc.9b02977.
(39) Hong, S. B.; Paik, W. C.; Lee, W. M.; Kwon, S. P.; Shin, C.-H.; Nam, I.-S.; Ha, B.-H. 02-P-10-Synthesis and Characterization of Zeolite ZSM-25. In *Studies in Surface Science and Catalysis*; Galarneau, A., Fajula, F., Di Renzo, F., Vedrine, J., Eds.; Elsevier, 2001; Vol. 135, p 186. https://doi.org/10.1016/S0167-2991(01)81349-5.
(40) Hu, X.; Brandani, S.; Benin, A. I.; Willis, R. R. Development of a Semiautomated Zero Length Column Technique for Carbon Capture Applications: Rapid Capacity Ranking of Novel Adsorbents. *Ind. Eng. Chem. Res.* **2015**, *54* (26), 6772–6780. https://doi.org/10.1021/acs.iecr.5b00513.
(41) Smith, J. M.; Van Ness, H. C.; Abbott, M. M. *Introduction to Chemical Engineering Thermodynamics*, 7th ed.; McGraw-Hill Education, 2004.
(42) Gmehling, J.; Kolbe, B.; Kleiber, M.; Rarey, J. *Chemical Thermodynamics for Process Simulation*, 1st ed.; Wiley-VCH Verlag, 2012.
(43) Duncan, W. L.; Möller, K. P. A 'Zero Length' Criterion for ZLC Chromatography. *Chem. Eng. Sci.* **2000**, *55* (22), 5415–5420. https://doi.org/10.1016/S0009-2509(00)00160-3.
(44) Gale, J. D. GULP: A Computer Program for the Symmetry-Adapted Simulation of Solids. *J. Chem. Soc. Faraday Trans.* **1997**, *93* (4), 629–637. https://doi.org/10.1039/A606455H.
(45) Rajendran, A.; Kariwala, V.; Farooq, S. Correction Procedures for Extra-Column Effects in Dynamic Column Breakthrough Experiments. *Chem. Eng. Sci.* **2008**, *63* (10), 2696–2706. https://doi.org/10.1016/j.ces.2008.02.023.
(46) Joss, L.; Mazzotti, M. Modeling the Extra-Column Volume in a Small Column Setup for Bulk Gas Adsorption. *Adsorption* **2012**, *18* (5), 381–393. https://doi.org/10.1007/s10450-012-9417-z.
(47) Brandani, S. A Simple Graphical Check of Consistency for Zero Length Column Desorption Curves. *Chem. Eng. Technol.* **2016**, *39* (6), 1194–1198. https://doi.org/10.1002/ceat.201500634.

(48) Mangano Enzo; Brandani Stefano; Ruthven Douglas M. Analysis and Interpretation of Zero Length Column Response Curves. *Chem. Ing. Tech.* **2013**, *85* (11), 1714–1718. https://doi.org/10.1002/cite.201300083.
(49) Buckingham, R. A.; Lennard-Jones, J. E. The Classical Equation of State of Gaseous Helium, Neon and Argon. *Proc. R. Soc. Lond. Ser. Math. Phys. Sci.* **1938**, *168* (933), 264–283. https://doi.org/10.1098/rspa.1938.0173.
(50) Chen, L.; Morrison, C. A.; Düren, T. Improving Predictions of Gas Adsorption in Metal–Organic Frameworks with Coordinatively Unsaturated Metal Sites: Model Potentials, Ab Initio Parameterization, and GCMC Simulations. *J. Phys. Chem. C* **2012**, *116* (35), 18899–18909. https://doi.org/10.1021/jp3062527.
(51) Vrabec, J.; Stoll, J.; Hasse, H. A Set of Molecular Models for Symmetric Quadrupolar Fluids. *J. Phys. Chem. B* **2001**, *105* (48), 12126–12133. https://doi.org/10.1021/jp012542o.